Charging dynamics of the electric double layer in porous media

Hidetsugu Sakaguchi and Reisei Baba
Department of Applied Science for Electronics and Materials, Interdisciplinary Graduate School of Engineering Sciences, Kyushu University, Kasuga, Fukuoka 816-8580, Japan

(Received 2 March 2007; revised manuscript received 10 April 2007; published 2 July 2007)

Electric double layer in porous media is studied with direct numerical simulations of the Nernst-Planck-Poisson equation. The time evolution of the charging process of the electric double-layer along a straight pore is first studied, and confirm that the time evolution obeys a power law of the exponent 1/2. We find that the diffusion constant increases effectively by the effect of the width of the pore. Next it is found that the time evolution of the charging process in fractal porous media obeys a power law, and the exponent α is related to the fracton dimension. Finally, we propose a coupled map lattice model for the creation of pore structures by gas activation processes, and perform numerical simulation of the charging dynamics of the electric double layer.

DOI: 10.1103/PhysRevE.76.011501 PACS number(s): 82.45.−h, 05.45.Df, 66.10.Cb

I. INTRODUCTION AND MODEL EQUATION

The electric double layer plays an important role in various research fields such as plasma physics, electrochemistry, and colloidal science. Electric double-layer capacitors (EDLCs) are electric devices with large capacitance using the electric double layer [1,2]. The high capacitance is caused by the large surface area in the random porous media such as the activated carbon. It is important to understand the electric double layer in random porous media. In the previous paper, we have studied the charging dynamics of the electric double layer on self-similar fractal electrodes using the Nernst-Planck-Poisson equation, and found a stretched exponential law for the charging dynamics [3]. There are open wide spaces around the fractal electrodes such as a diffusion-limited aggregation (DLA) cluster or a critical percolation cluster, in which ions can diffuse rather freely. However, ions need to diffuse through long narrow pores in the porous media. It takes therefore rather long time for ions to spread out the porous media, and the charging dynamics is expected to become very slow.

The slow relaxation of the charging process is closely related to the anomalous behavior of the impedance. The constant-phase angle (CPA) impedance, which has a form of $Z(\omega)=R+k(i\omega)^{-p}$, has been known in various media since 1920s. Levie proposed a transmission line model with $p=1/2$ for porous electrodes [4]. Sapoval, Pajkossy-Nyikos, and Leibig-Halsey studied the CPA impedance for fractal electrodes, and showed the exponent p is related the fractal dimension D_f [5–8]. The CPA impedance was also studied experimentally by Larsen *et al.* and Pajkossy-Kyikos [9,10]. Sanabria and Miller studied nonporous electrodes of stainless steel, proposed an overdamped oscillator model for the impedance, and they suggested the importance of the CPA impedance only for obviously porous electrodes [11].

The impedance $Z(\omega)$ is related to the relaxation function of the current $I(t)=dQ(t)/dt$ for the stepwise electrode potential $\phi=V\theta(t)$ [$\theta(t)$ is the Heaviside step function] as $I(\omega)=V/[i\omega Z(\omega)]$, where $I(\omega)=\int_0^\infty I(t)e^{-i\omega t}dt$. If $Q(t)\sim t^\alpha$ and $I(t)\sim t^{\alpha-1}$, $I(\omega)=\int_0^\infty t^{\alpha-1}e^{-i\omega t}dt=\omega^{-\alpha}\int_0^\infty t'(\alpha-1)e^{-it'}dt'\sim\omega^{-\alpha}$. Therefore, the power law type of slow relaxation in porous media is directly related to the CPA impedance, that is, $\alpha\sim p$. However, the CPA impedance or the slow relaxation characterized by the power law decay was not explicitly studied in the Nernst-Planck-Poisson equation.

In this paper, we study the electric double layer by the direct numerical simulation of the Nernst-Planck-Poisson equation, which is a dynamical version of the Gouy-Chapman model [12,13]. In the Gouy-Chapman model, the electric double layer is constructed only with the diffusion double layer. The electric potential obeys the Poisson equation. Positive and negative ions satisfy the Nernst-Planck equations. In this paper, we do not consider various effects such as finite-length-dipole effects, nonlinear effects by large V, and steric effects of finite ion size, although they are important in realistic EDLCs [14–16]. Although there are several limitations in the Nernst-Planck-Poisson equation as discussed in Ref. [16], the Nernst-Planck-Poisson equation is a simple and basic model, and the dynamical behaviors of the equation in complicated media have not been investigated in detail. We will study the charging dynamics of electric double-layer in porous media using the Nernst-Planck-Poisson equation.

The Nernst-Planck-Poisson equations are written as

$$\frac{\partial\rho_+}{\partial t}=D_+\nabla^2\rho_+ + \mu_+ e\,\nabla\,(\rho_+\,\nabla\,\phi),$$

$$\frac{\partial\rho_-}{\partial t}=D_-\nabla^2\rho_- - \mu_- e\,\nabla\,(\rho_-\,\nabla\,\phi), \tag{1}$$

$$\nabla^2\phi=\frac{e}{\epsilon}(\rho_- - \rho_+), \tag{2}$$

where ϕ is the electric potential, ρ_+ and ρ_- denote the concentration of the positive and negative ions, $D_\pm$ denotes the diffusion constant for ions, $\mu_\pm$ is the mobility of ions, and ϵ is the dielectric constant. We assume further that the charge of each ion is $\pm e$, and the mobility of each ion is the same $\mu_+=\mu_-=\mu$ for the sake of simplicity. Owing to the Einstein relation, the diffusion constant and the mobility satisfy the relation $D_+=D_-=D=\mu k_B T$. By rescaling of the space and

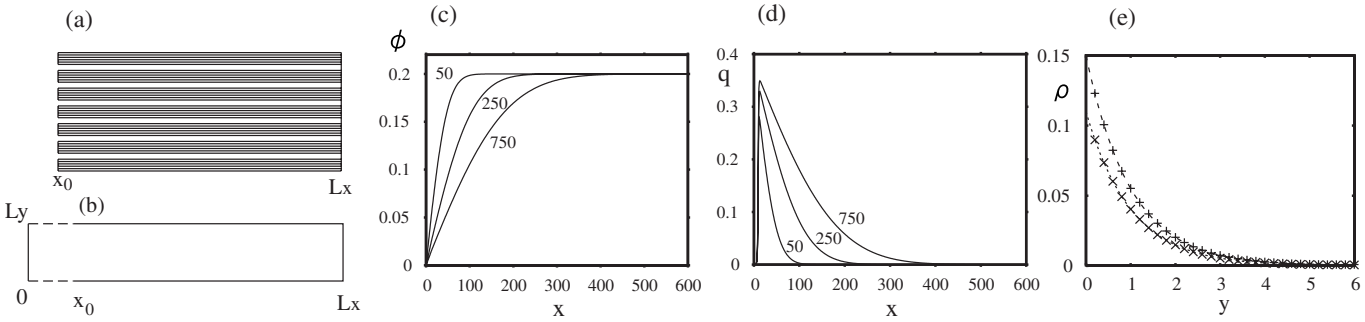

FIG. 1. (a) Porous medium with parallel straight pores. (b) One straight rectangular pore. (c) Snapshot profiles of $\phi(x,L_y/2,t)$ at $t=50$, 500, and 750 for $L_x=600$, $L_y=12$, $x_0=10$, $V=0.2$, $T=2$, and $\rho_0=1$. (d) Snapshot profiles of $q(x,t)$ at $t=50$, 250, and 750. (e) Snapshot profiles of $\rho(x,y)=\rho_-(x,y,t)-\rho_+(x,y,t)$ at $x=15$ and 60 as a function of y at $t=750$.

time coordinates and the electric potential using the Debye length $\lambda_s=[\epsilon k_B T_s/(e^2\rho_s)]^{1/2}$, $t_s=\epsilon/(\mu e^2\rho_s)$, and $V_s=k_BT_s/e$ at a certain temperature T_s and a certain concentration ρ_s, Eqs. (1) and (2) are rewritten as

$$\frac{\partial \rho_+}{\partial t} = T\nabla^2\rho_+ + \nabla(\rho_+ \nabla \phi),$$

$$\frac{\partial \rho_-}{\partial t} = T\nabla^2\rho_- - \nabla(\rho_- \nabla \phi), \tag{3}$$

and

$$\nabla^2\phi = \rho_- - \rho_+. \tag{4}$$

We assume that there is a flat electrode at $x=0$, and a long porous medium is located for $x>x_0$, which is sharply cut at x_0 as shown in Fig. 1(a). The ion concentration is fixed to be ρ_0 and the electric potential ϕ is 0 at the flat electrode $x=0$. The electric potential is fixed to be V at the porous medium, which acts as anode. The control parameters are the dimensionless temperature T, the electrode potential V at the porous media, and the concentration ρ_0. Periodic boundary conditions are assumed in the y direction, that is, $\phi(x,L_y)=\phi(x,0)$, $\rho_+(x,L_y)=\rho_+(x,0)$, and $\rho_-(x,L_y)=\rho_-(x,0)$. When the electrode potential V is sufficiently small, the system becomes a linear system and Eq. (3) is approximated as

$$\frac{\partial \rho_+}{\partial t} = T\nabla^2\rho_+ + \nabla(\rho_0 \nabla \phi),$$

$$\frac{\partial \rho_-}{\partial t} = T\nabla^2\rho_- - \nabla(\rho_0 \nabla \phi). \tag{5}$$

II. ELECTRIC DOUBLE-LAYER AROUND A STRAIGHT POROUS ELECTRODE

First, we consider a simple porous medium constructed of straight parallel pores as shown in Fig. 1(a). We study an even simpler system in which the anode is constructed of only one straight rectangular pore of width L_y and length L_x-x_0, as shown in Fig. 1(b). The electric potential is fixed to be $\phi=V$ at $y=0$, $y=L_y$ for $x_0<x<L_x$, $x=L_x$, and $\phi=0$ at $x=0$. The initial conditions are $\rho_+=\rho_-=\rho_0$ and $\phi=0$ except for the boundaries. We have performed direct numerical simulation of Eqs. (3) and (4) with the Euler method with grid size $\Delta x=0.2$ and time step $\Delta t=0.001$. The charge density per unit length in the x direction is expressed as $q(x,t)=\int_0^{L_y}[\rho_-(x,y,t)-\rho_+(x,y,t)]dy$, and the total charge is expressed as $Q(t)=\int_0^{L_x}q(x,t)dx$. Figures 1(c) and 1(d) display, respectively, three snapshot profiles of $\phi(x,y,t)$ at $y=L_y/2$ and $q(x,t)$ at $t=50$, 250, and 750 for $L_x=600$, $L_y=12$, $x_0=10$, $V=0.2$, $T=2$, and $\rho_0=1$. As the charge is stored, the electric potential $\phi(x,L_y/2)$ decreases gradually from $V=0.2$ to 0, which is seen from Figs. 1(c) and 1(d). Figure 1(e) displays profiles of $\rho(x,y)=\rho_-(x,y,t)-\rho_+(x,y,t)$ at $x=15$ and 60 as a function of y at $t=750$. The profiles of the stored charge $\rho(x,y,t)$ is well approximated by the exponential function $0.15\exp(-y)$ $(x=15)$ and $0.11\exp(-y)$ $(x=60)$. Note that the relaxation constant of the exponential decay is equal to the Debye length $\lambda=\sqrt{T/(2\rho_0)}=1$. These results suggest that the electric potential $\phi(x,y,t)$ is expressed as

$$\phi(x,y,t) = \phi_0(x,t) + \delta\phi(x,y,t), \tag{6}$$

where $\phi_0(x,t)\sim\phi(x,L_y/2,t)$, and

$$\rho_\pm(x,y,t) = \rho_0[1 \mp \delta\phi(x,y,t)]/T. \tag{7}$$

Here $\phi_0(x,t)$ can be assumed to be a constant, when we consider the profiles of $\rho_\pm$ and ϕ in the y direction. Then, the Poisson equation is approximated as

$$\nabla^2\phi \sim \frac{\partial^2\phi}{\partial y^2} = \frac{\partial\delta\phi}{\partial y^2} = \frac{2\rho_0}{T}\delta\phi, \tag{8}$$

because the spatial variation in the x direction is very small, i.e., $|\partial\phi/\partial x| \ll |\partial\phi/\partial y|$. Hence, $\delta\phi$ is expressed as

$$\delta\phi = \delta\phi_0 \cosh[(y-L_y/2)/\lambda], \tag{9}$$

where

$$\delta\phi_0 = [V-\phi_0(x,t)]/\cosh[L_y/(2\lambda)],$$

by the boundary conditions: $\phi(x,0,t)=\phi(x,L_y,t)=V$. The stored charge density $q(x,t)$ is expressed as

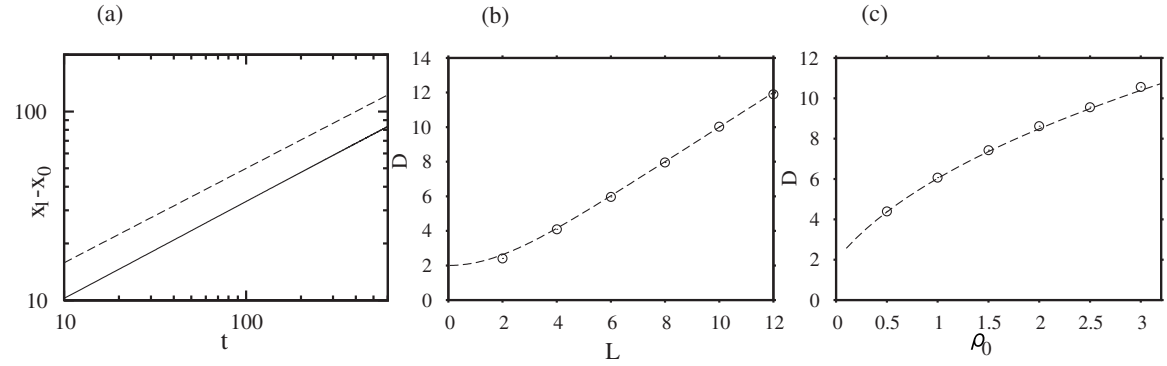

FIG. 2. (a) Distance x_1-x_0, where the charge density $q(x,t)$ becomes half of the maximum value as a function of t. The dashed line denotes a line of $x_1-x_0 \sim t^{1/2}$. (b) Effective diffusion constant D as a function of L_y evaluated from direct numerical simulation and the theoretical curve by Eq. (12). (c) Effective diffusion constant D as a function of ρ_0 evaluated from direct numerical simulation and the theoretical curve by Eq. (12).

$$q = \frac{2\rho_0[V-\phi_0(x,t)]}{T\cosh[L_y/(2\lambda)]}\int_0^{L_y}\cosh[(y-L_y/2)/\lambda]dy$$

$$= \frac{2[V-\phi_0(x,t)]\tanh[L_y/(2\lambda)]}{\lambda}. \quad (10)$$

In the equilibrium state, $\phi_0(x,t)=0$ if $L_y/2 \gg \lambda$, and the total charge is expressed as

$$Q \sim \int_{x_0}^{L_x} q(x,t)dx = 2V\tanh[L_y/(2\lambda)](L_x-x_0),$$

and the capacity per unit length is expressed as

$$C = 2\tanh[L_y/(2\lambda)]/\lambda.$$

In the charging process, $\phi_0(x,t)$ is not zero as shown in Fig. 1(c), but the charge density $q(x,t)$ is approximately expressed as $q(x,t)=C[V-\phi_0(x,t)]$, or $V-\phi_0(x,t)=q(x,t)/C$, and

$$\delta\phi = \frac{[V-\phi_0(x,t)]\cosh[(y-L_y/2)/\lambda]}{\cosh[L_y/(2\lambda)]}.$$

By the integral of Eq. (5) with respect to y, $q(x,t)$ obeys

$$\frac{\partial q}{\partial t} = T\frac{\partial^2 q}{\partial x^2} - 2\rho_0\frac{\partial^2}{\partial x^2}\int_0^{L_y}\phi(x,y,t)dy = T\frac{\partial^2 q}{\partial x^2}$$

$$- 2\rho_0\frac{\partial^2}{\partial x^2}\{\phi_0(x,t)L_y + [V-\phi_0(x,t)]\lambda\tanh[L_y/(2\lambda)]\}$$

$$= T\frac{\partial^2 q}{\partial x^2} - 2\rho_0\frac{\partial^2}{\partial x^2}\{[V-q(x,t)/C]L_y$$

$$+ q(x,t)/C\lambda\tanh[L_y/(2\lambda)]\} = D\frac{\partial^2 q}{\partial x^2}, \quad (11)$$

where

$$D = \frac{\rho_0\lambda L_y}{\tanh[L_y/(2\lambda)]}. \quad (12)$$

This implies that the charge density $q(x,t)$ obeys a diffusion equation with the effective diffusion constant D. A solution of Eq. (11) for $x>x_0$ and $L_x \gg 1$ is approximated as

$$q(x,t) = \frac{2q_0}{\sqrt{\pi}}\left(\frac{\sqrt{\pi}}{2} - \int_0^{x'}\exp(-z^2)dz\right), \quad (13)$$

where $x'=(x-x_0)/(2\sqrt{Dt})$ and $q_0 \sim CV$. The stored charge density $q(x,t)$ decays as in Fig. 1(d), as a function of x. We can evaluate the position x_1, where the charge density $q(x,t)$ becomes half of the maximum value $q_{\max}$ at each time. Figure 2(a) displays the distance x_1-x_0 from the edge at $x=x_0$ of the pore as a function of t. The distance x_1-x_0 increases as $x_1-x_0=0.954\sqrt{D}t^{1/2}$ for the solution (13). We can evaluate the effective diffusion constant D from Fig. 2(a) as $D=3.29$. We have evaluated the effective diffusion constant D as a function of L_y for $T=2$ and $\rho_0=1$. The results are shown in Fig. 2(b). The dashed curve is obtained from Eq. (12). As L_y is decreased, D approaches $T=2$. For large L_y, D increases in proportion to L_y. That is, the diffusion constant increases effectively in a wide pore. Figure 2(c) displays the effective diffusion constant evaluated from numerical simulations as a function of ρ_0 for $L_y=6$ and $T=2$. The dashed curve denotes Eq. (12). Thus, we have found that the charging dynamics around a straight pore is well described by the diffusion equation with a diffusion constant different from the original diffusion constant T. The total charge $Q(t)=\int_{x_0}^{L_x}q(x,t)dx$ also increases as $Q(t)\sim Dt^{1/2}$ if L_x is sufficiently large. The power law relaxation with the exponent 1/2 is the same as the model by Levie, but the effective diffusion constant was not evaluated before [4].

III. CHARGING DYNAMICS OF ELECTRIC DOUBLE-LAYER AROUND FRACTAL POROUS ELECTRODES

In the previous section, we found that the width of the pore changes the diffusion constant effectively but the time evolution of the exponent $\alpha=1/2$ does not change by the width of the pore. In this section, we will investigate more intricate fractal pore networks. One is a critical percolation cluster and the other is a DLA cluster. In the previous paper, we have used these fractals as the electrodes and found a stretched exponential relaxation. In this paper, we use these

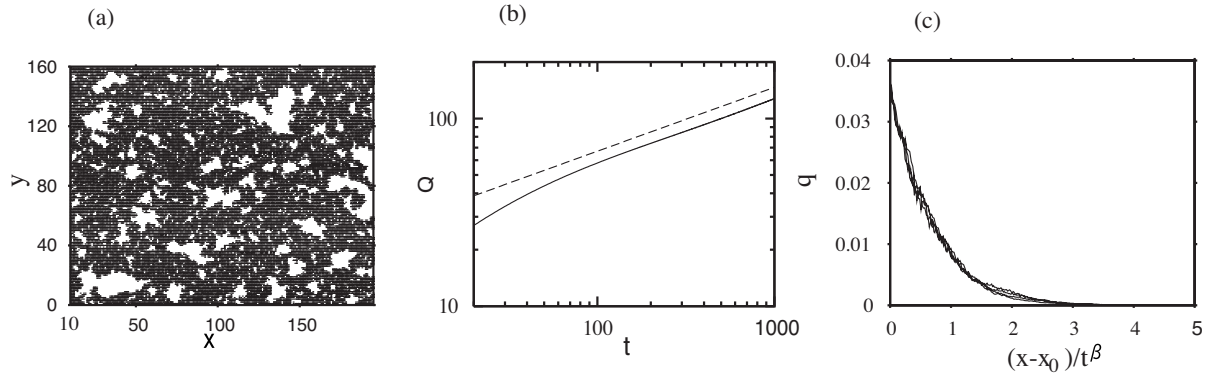

FIG. 3. (a) Critical percolation cluster. (b) Time evolution of the total charge $Q(t)$. The dashed line denote $Q \sim t^{0.34}$. (c) Four snapshot profiles of $q(x,t)$ as a function of $\tilde{x}=(x-x_0)/t^{0.35}$ at $t=400$, 800, 1200, and 1600.

fractals as pores, through which ions diffuse, and the space other than the pore area is considered to be the electrode. We have performed numerical simulations in a box of $L_x=200$, $x_0=10$, and $L_y=160$ for $T=2$, $V=0.2$, and $\rho_0=1$. Figure 3(a) displays a critical percolation cluster. The critical percolation cluster is cut at x_0, and the ions diffuse into the percolation cluster from $x=x_0$. Figure 3(b) displays the time evolution of the total charge $Q(t)$. The total charge grows as $Q \sim t^{\alpha}$ with $\alpha \sim 0.34$. The average charge density $q(x,t)$ at x was calculated as $q(x,t)=\Sigma_{y=0}^{L_y}[\rho_-(x,y,t)-\rho_+(x,y,t)]/\Sigma_{y=0}^{L_y}1(x,y)$, where $1(x,y)$ takes 1 if the site at (x,y) is included in the percolation cluster. Figure 3(c) displays $q(x,t)$ as a function of $\tilde{x}=(x-x_0)/t^{\beta}$ with $\beta=0.35$ at $t=400$, 800, 1200, and 1600. The fairly good overlap implies that a scaling law with the exponent β is satisfied for the average charge density. Figure 4(a) displays a DLA cluster, which had grown from a linear seed at $x=x_0$. The ions diffuse on the DLA cluster from $x=x_0$. The initial concentration is $\rho_+=\rho_-=\rho_0$ on the DLA cluster and in the region $x<x_0$. Figure 4(a) displays a time evolution of the total charge $Q(t)$. The total charge grows as $Q \sim t^{\alpha}$ with $\alpha \sim 0.32$. The average charge density $q(x,t)$ at x was similarly calculated as $q(x,t)=\Sigma_{y=0}^{L_y}[\rho_-(x,y,t)-\rho_+(x,y,t)]/\Sigma_{y=0}^{L_y}1(x,y)$, where $1(x,y)$ takes 1 if the site is included in the DLA cluster. Figure 4(c) displays $q(x,t)$ as a function of $\tilde{x}=(x-x_0)/t^{\beta}$ with $\beta=0.37$ at $t=500$, 1000, 1500, and 2000. The fairly good overlap implies a scaling law with the exponent β is satisfied for the average charge density also in the DLA pore network.

The charging dynamics around the fractal pore network is closely related to the diffusion on the fractal network. It is expected that the characteristic exponent for the charging dynamics of the electric double layer is essentially the same as the one for the diffusion, as seen from the previous section. The diffusion on the fractal network has been intensively studied [17]. The anomalous diffusion occurs on the fractal network. The mean square distance R^2 of a random walker starting from a certain point is scaled as t^{2/d_w}, where d_w is the anomalous diffusion exponent. For a loopless fractal such as the DLA cluster, d_w is given by D_f+1 [17,18]. For the DLA cluster, $D_f \sim 1.71$ and $d_w \sim D_f+1=2.71$. The total charge $Q(t)$ is roughly estimated as $Q \sim R^{D_f} \sim t^{D_f/d_w}$, if the ions diffuse from a certain point. The exponent $D_s=2D_f/d_w$ is called the fracton dimension. The fracton dimension for the DLA cluster is therefore $D_s=2\times 1.71/2.71 \sim 1.26$. The fracton dimension for the critical percolation cluster is $D_s \sim 4/3$, which is called the Alexander-Orbach conjecture [19]. On the other hand, the fractal dimension of the critical percolation cluster is $D_f=91/48$ and therefore $d_w \sim 2.87$. If ions diffuse into porous media from a line as our porous media, the exponent is expected to become half of the exponent for the case from a point. The total charge is therefore expected to obey $Q \sim t^{D_s/4}$. One of the authors investigated an adsorption-diffusion process on the fractal network and confirmed that the total adsorbent quantity obeys $Q(t) \sim t^{D_s/4}$ and the scaling law for the concentration $\rho(x,t)$ is approximated by $\rho[(x-x_0)/t^{\beta}]$ with $\beta=1/d_w$ [20]. Our problem of the charging dynamics of the electric double-layer is

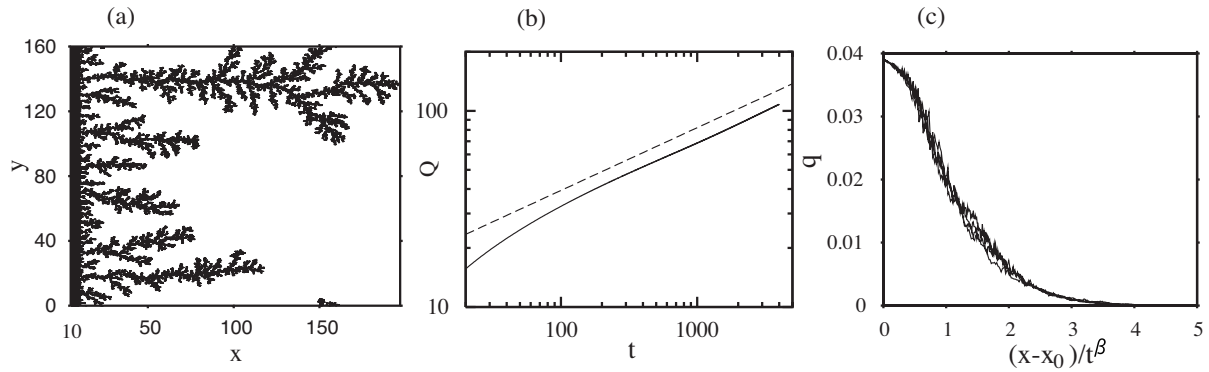

FIG. 4. (a) DLA cluster. (b) Time evolution of the total charge $Q(t)$. The dashed line denote $Q \sim t^{0.32}$. (c) Four snapshot profiles of $q(x,t)$ as a function of $\tilde{x}=(x-x_0)/t^{0.39}$ at $t=500$, 1000, 1500, and 2000.

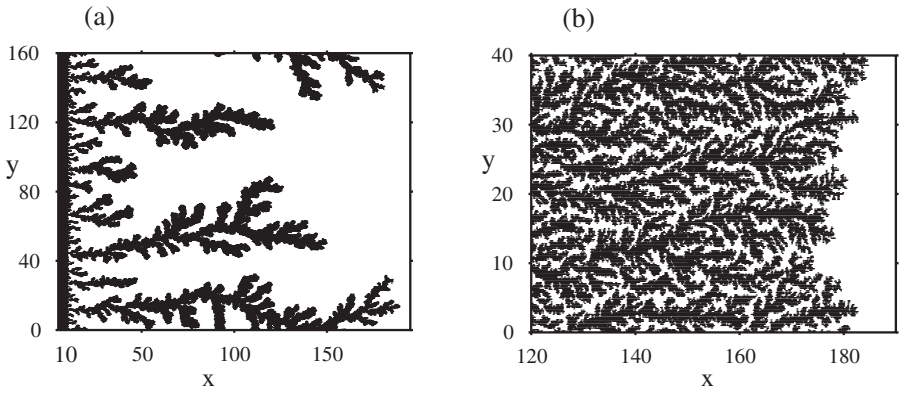

FIG. 5. (a) DLA-like pore pattern generated by a coupled map lattice with $\Delta u=6$. (b) DBM-like pore pattern generated by a coupled map lattice with $\Delta u=2$.

different for the adsorption-diffusion problem, however, the same scaling law is expected to be satisfied, because the anomalous diffusion on the fractal network is essential in both problems. Actually, the numerically obtained exponent $\alpha=0.32$ for the DLA cluster is close to $D_s/(2d_w)=1.7/(2\times2.7)=0.315$ and the exponent $\alpha=0.34$ for the critical percolation cluster is close to $D_s/(2d_w)=0.33$. The exponent $\beta=0.35$ for the critical percolation cluster is close to the exponent $1/d_w=1/2.87\sim0.348$, and the exponent $\beta=0.39$ for the DLA cluster is also close to $1/d_w=1/2.7\sim0.37$. Thus, we have found that the exponent α is not directly related to the fractal dimension D_f in our model, but it is related to the fracton dimension, which was not noticed in previous studies [5–8].

IV. ELECTRIC DOUBLE-LAYER IN POROUS MEDIA GENERATED BY A COUPLED MAP LATTICE MODEL

Activated carbon is used as electrode materials in EDLCs. An activation process by hot water vapor is often used to generate many micro pores in carbon material. The chemical reactions for the gas activation process are expressed as

$$C + H_2O \rightarrow CO + H_2,$$

$$C + 2H_2O \rightarrow CO_2 + 2H_2.$$

The solid carbon changes into the gases: CO, H_2, and CO_2 by the reactions and evaporates from the interface of the solid and the gas. As a result of the evaporation, micropores are created, although the detailed processes of the pore creation are not well understood now. These reactions are endothermic. The high temperature is necessary for the reactions, but the temperature is decreased owing to the endothermic reaction, when the chemical reactions proceed. The situation is similar to the melt growth of crystal, although the supercooling is necessary for the growth, the latent heat is released by the growth, and therefore the effect of the temperature is reversed, in the case of the melt growth. A kind of the Mullins-Sekerka instability is expected to occur under these conditions and the flat surface might be unstable [21]. This is a possible origin of the growth of micropores. We proposed a coupled map lattice model for the melt growth and found various patterns such as DLAs, dendrites, and dense branching patterns (DBM) in the coupled map lattice models [22–24]. We can construct a coupled map lattice model for the activation process of carbon.

In the coupled map lattice model, there are two variables at each lattice site on a square lattice; one variable u denotes the temperature and the other variable p is an order parameter, which indicates the degree of the vaporization at each lattice site. The order parameter p takes 0 at solid sites and increases according to the chemical reaction at the interface sites. The interface sites are located in the nearest neighbor sites and the next-nearest-neighbor sites of solid sites. The time evolutions are performed in two steps on each lattice point. The first step is a diffusion process expressed as

$$u_n'(i,j) = u_n(i,j) + D/\Delta x^2[u_n(i+1,j) + u_n(i-1,j) + u_n(i,j+1) + u_n(i,j-1) - 4u_n(i,j)], \quad (14)$$

where u is a dimensionless temperature, n is an integer step number, Δx is the grid size, D is the diffusion constant, and the time step $\Delta t=1$ is assumed. We have assumed the parameter values as $\Delta x=0.2$ and $D=0.008$. The second step is an evaporation process, which occurs only at the interface sites. At the nearest neighbor sites of solid sites, the second step is expressed as

$$p_{n+1}(i,j) = p_n(i,j) + \gamma[u_n'(i,j)],$$

$$u_{n+1}(i,j) = u_n'(i,j) - \Delta u\,\gamma[u_n'(i,j)], \quad (15)$$

and at the next-nearest-neighbor sites of solid sites, the second step is expressed as

$$p_{n+1}(i,j) = p_n(i,j) + c\,\gamma[u_n'(i,j)],$$

$$u_{n+1}(i,j) = u_n'(i,j) - c\Delta u\,\gamma[u_n'(i,j)], \quad (16)$$

where $\gamma(u)$ represents the reaction rate constant and it is assumed to be $\gamma(u)=0.5\exp[-1/u(i,j)]$ by Arrhenius's law, $-\Delta u$ is proportional to the heat of reaction, and $c=0.35$ is used in our simulation to reduce the anisotropy effect of the square lattice. If the variable p reaches a threshold value $p_c(i,j)$, the lattice site is assumed to be completely evaporated, the lattice site changes into a gas site, and the interface moves by one site. Because the carbon material is rather random, we have further assumed that the threshold value $p_c(i,j)$ is randomly distributed between 0.2 and 1. Owing to

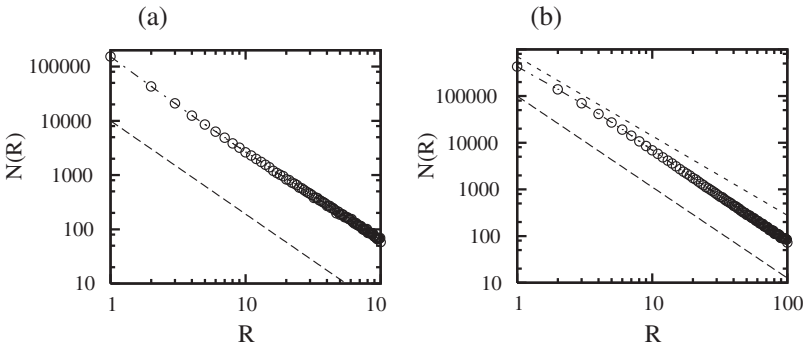

FIG. 6. (a) Double logarithmic plot of the box number $N(R)$ vs the length scale R for the DLA-like pore pattern shown in Fig. 5(a). The dashed line corresponds to the fractal dimension 1.72. (b) Double logarithmic plot of $N(R)$ vs R for the DBM-like pore pattern shown in Fig. 5(b). Two dashed lines correspond to the dimension 1.95 and 1.7.

this effect of the random threshold, DLA-like or DBM-like random patterns appear. The initial condition is $p(i,j)=0$ for $x=i\Delta x>x_0=10$ and the temperature $u(i,j)=1$ at every site. Figure 5(a) displays a DLA-like pore pattern for $\Delta u=6$ obtained by a numerical simulation of the coupled map lattice, where the shaded region denotes a pore region where the order parameter p has gone over the threshold $p_c(i,j)$. Figure 5(b) displays a DBM-like pore pattern for $\Delta u=2$. Because the pattern has a fine structure, we have shown only a region in $120<x<190$ and $0<y<40$. As the parameter Δu is increased, the decrease of the temperature by the chemical reaction is larger, and the chemical reaction tends to be strongly suppressed. As a result, a DLA-like pore pattern grows as Fig. 5(a). We have calculated the fractal dimension of the patterns by the standard box counting method. Figure 6(a) displays a double-logarithmic plot of the box number N as a function of the length scale R for the pattern in Fig. 5(a). The fractal dimension is estimated as $D_f\sim 1.72$. Figure 6(b) displays a double-logarithmic plot of the box number N vs R for the pattern in Fig. 5(b). Two dashed lines denote the lines of the exponent $D_f=1.7$ and $D_f=1.95$. The curve of $N(R)$ is slightly curved in the smaller scale region, the fractal dimension in the smaller scale is $D_f\sim 1.7$, which is close to the dimension of the DLA cluster, and however, the fractal dimension in the larger scale is $D_f\sim 1.95\sim 2$, which implies a dense pattern.

We have performed numerical simulation of the charging dynamics of the electric double-layer by Eqs. (3) and (4) using the porous media generated by the coupled map lattice model. Figures 7(a) and 7(b) display the time evolutions of the total charge $Q(t)$ for the DLA-like and DBM-like pore patterns. The total charge $Q(t)$ increases as $Q(t)\sim t^{0.33}$ for the DLA-like pore pattern in Fig. 5(a). The exponent $\alpha=0.33$ is close to the value 0.315, which is expected for the DLA pattern. The total charge $Q(t)$ increases as $Q(t)\sim t^{0.45}$ for the DBM-like pore pattern shown in Fig. 5(b). The exponent $\alpha=0.45$ is rather large compared the value $1.95/(2\times 2.95)\sim 0.33$, which is expected for the loopless fractal pattern with fractal dimension $D_f=1.95$. The exponent 0.45 is between the value 0.33 expected for a loopless fractal pattern with $D_f=1.95$ and 0.5 for a straight pore. We do not understand the reason well now, but it might be related to the facts that the pore density is large and the pore width cannot be negligible, and the effect of the branching structure becomes weak.

V. SUMMARY

We have studied the charging dynamics of the electric double-layer in porous media with direct numerical simulations of the Nernst-Planck-Poisson equation. The electrode potential is assumed to be relatively small, in which the linear relation is satisfied. First, we have confirmed that the time evolution of the stored charge obeys a power law of the exponent 0.5. We have found that the effective diffusion constant changes with the width L_y of the pore, but the characteristic exponent α does not change with L_y. Next, we have studied the charging dynamics in fractal porous media. The charging dynamics obeys a power law and the exponent is related to the fracton dimension. Finally, we have proposed a coupled map lattice model for the pore creation in carbon material. DLA-like or DBM-like patterns appear as a result of a kind of the Mullins-Sekerka instability. The charging dynamics has been investigated for the porous media generated by the coupled map lattice using the Nernst-Planck-Poisson equation. The charging dynamics obeys a power law. The exponent is consistent to the fracton dimension for the

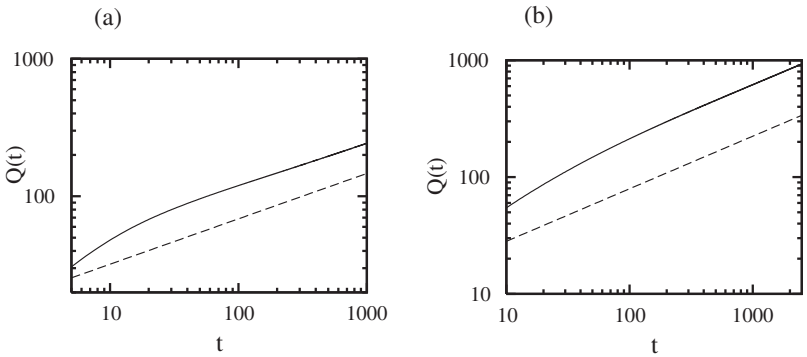

FIG. 7. (a) Time evolution of the total charge $Q(t)$ for the DLA-like pore pattern shown in Fig. 5(a). The dashed line denotes a power law of exponent 0.33. (b) Time evolution of the total charge $Q(t)$ for the DBM-like pore pattern shown in Fig. 5(b). The dashed line denotes a power law of exponent 0.45.

DLA-like pattern. As the pore density is increased, DLA-like patterns changes into DBM-like patterns, and the exponent α increases toward the value of the straight pore.

As explained in the first section, we have not considered various effects such as nonlinear effects by large V, the Helmholtz layer, and steric effects of finite ion size for the charging dynamics, in this paper. The nonlinear effect by large V and some effects of the Helmholtz layer might be investigated in some generalized models of the Nernst-Planck-Poisson equation [16], which are left as future problems. However, there are also various effects such as finite size effects or discreteness of ions, some of which might be difficult to study in continuum models like the generalized Nernst-Planck-Poisson equations, and other numerical methods such as the molecular dynamics simulation might be necessary.

[1] S. Sarangapani, B. V. Tilak, and C. P. Chen, J. Electrochem. Soc. **143**, 3791 (1996).
[2] B. E. Conway, V. Birss, and J. Wojtowicz, J. Power Sources **66**, 1 (1997).
[3] H. Sakaguchi and R. Baba, Phys. Rev. E **75**, 051502 (2007).
[4] R. De Levie, Electrochim. Acta **9**, 1231 (1964).
[5] B. Sapoval, Solid State Ionics **23**, 253 (1987).
[6] L. Nyikos and T. Pajkossy, Electrochim. Acta **30**, 1533 (1985).
[7] M. Leibig and T. C. Halsey, Electrochim. Acta **38**, 1985 (1993).
[8] T. C. Halsey and M. Leibig, Phys. Rev. A **43**, 7087 (1991).
[9] A. E. Larsen, D. G. Grier, and T. C. Halsey, Phys. Rev. E **52**, R2161 (1995).
[10] T. Pajkossy and L. Nyikos, Electrochim. Acta **34**, 171 (1989).
[11] H. Sanabria and J. H. Miller, Jr., Phys. Rev. E **74**, 051505 (2006).
[12] G. Gouy, J. Phys. (Paris) **9**, 457 (1910).
[13] D. L. Chapman, Philos. Mag. **25**, 475 (1913).
[14] J. Ross Macdonald and S. Kenkel, J. Chem. Phys. **80**, 2168 (1984).
[15] M. Z. Bazant, K. Thornton, and A. Ajdari, Phys. Rev. E **70**, 021506 (2004).
[16] M. S. Kilic, M. Z. Bazant, and A. Ajdari, Phys. Rev. E **75**, 021502 (2007).
[17] S. Havlin and D. Ben-Avraham, Adv. Phys. **36**, 695 (1987).
[18] S. Havlin and H. Wessman, J. Phys. A **19**, L1021 (1986).
[19] S. Alexander and R. Orbach, J. Phys. (Paris), Lett. **43**, L625 (1982).
[20] H. Sakaguchi, J. Phys. Soc. Jpn. **74**, 2703 (2005).
[21] W. W. Mullins and R. F. Sekerka, J. Appl. Phys. **34**, 323 (1963).
[22] H. Sakaguchi, J. Phys. Soc. Jpn. **67**, 96 (1998).
[23] H. Sakaguchi and M. Ohtaki, J. Phys. Soc. Jpn. **73**, 1723 (2004).
[24] H. Sakaguchi, K. Kishinawa, K. Katsuki, and H. Honjo, Phys. Rev. E **75**, 021606 (2007).